Available online at www.sciencedirect.com

SciVerse ScienceDirect

Ceramics International 39 (2013) 3603–3611

CERAMICS INTERNATIONAL

www.elsevier.com/locate/ceramint

Effect of preparation route on the microstructure and electrical conductivity of co-doped ceria

Dusan Bucevac[a,*], Aleksandar Radojkovic[b], Miroslav Miljkovic[c], Biljana Babic[a], Branko Matovic[a]

[a]*Institute of Nuclear Sciences Vinca, University of Belgrade, P.O. Box 522, 11001 Belgrade, Serbia*
[b]*Institute for Multidisciplinary Research, University of Belgrade, Kneza Viseslava 1, 11000 Belgrade, Serbia*
[c]*Center of Electron Microscopy, University of Nis, Bulevar Dr Zorana Djindjica 81, 18000 Nis, Serbia*

Received 20 August 2012; received in revised form 26 September 2012; accepted 10 October 2012
Available online 23 October 2012

Abstract

Dense $Ce_{0.8}Sm_{0.1}Gd_{0.1}O_{2-\delta}$ electrolytes were fabricated by sintering of CeO_2 solid solutions which were prepared from metal nitrates and NaOH using self propagating room temperature synthesis (SPRT). Three different routes were employed to obtain CeO_2 solid solution powders: (I) hand mixing of reactants, (II) ball milling of reactants and (III) ball milling of $Ce_{0.8}Sm_{0.2}O_{2-\delta}$ and $Ce_{0.8}Gd_{0.2}O_{2-\delta}$ solid solutions previously prepared by ball milling of corresponding nitrates and NaOH. Density measurements showed that ball milling, which is more convenient than hand mixing, is an effective way to obtain almost full dense samples after presureless sintering at 1550 °C for 1 h. These samples had larger grain size and consequently higher conductivity than the samples obtained by hand mixing. The highest conductivity of 2.704×10^{-2} $(\Omega\,cm)^{-1}$was measured at 700 °C in a sample prepared by route II. It was found that reduced grain size in samples obtained by hand mixing leads to a decrease in grain boundary conductivity and therefore decrease in the total conductivity. The results showed that mixing of single doped ceria solid solutions improved densification and inhibited grain growth.

Keywords: A. Sintering; C. Ionic conduction; Ceria; Microstructure

1. Introduction

Solid oxide fuel cells (SOFCs) are power generation devices that convert chemical energy of fuels such as H_2, CH_4 or CO into electrical energy. The conversion normally involves fuel oxidation on anode and oxygen reduction on cathode [1]. In order to obtain an electron flow from the anode to the cathode it is essential that the fuel and oxygen are physically separated. This is accomplished by placing a solid electrolyte between the electrodes which prevents fuel-oxygen contact and at the same time allows transport of oxygen ions from the cathode to the anode. The oxygen transport is necessary for continuous oxygen supply to the anode and therefore continuous operation of SOFCs. One of the most successful electrolytes for application in SOFCs is doped ceria (CeO_2) which posses relatively high oxygen ionic conductivity at intermediate temperatures (500–700 °C) [2,3]. This temperature is considerably lower than 900 °C which is the operation temperature of mainly used SOFCs with yttria-stabilized zirconia (YSZ) electrolyte [4]. High oxygen ionic conductivity of ceria is ascribed to relatively open cubic fluorite structure which can accommodate wide range of concentrations of aliovalent cations such as rare earth (Re) cations (Yb^{3+}, Nd^{3+}, Dy^{3+}, Gd^{3+} and Sm^{3+}) [5]. The substitution of Ce^{4+} cations by Re^{3+} cations introduces vacancies in the oxygen sublattice as charge compensation defects [6]. This allows oxygen ions created on the cathode to hop through the vacancies and reach the anode.

In general, the conductivity of an electrolyte strongly depends on the size and concentration of dopant cation [7,8]. Besides these parameters, which are considered as intrinsic properties of material itself, there are parameters which are dependent on preparation route and sintering conditions. For example, density and grain size, which are

*Corresponding author.
E-mail address: bucevac@vinca.rs (D. Bucevac).

0272-8842/$ - see front matter © 2012 Elsevier Ltd and Techna Group S.r.l. All rights reserved.
http://dx.doi.org/10.1016/j.ceramint.2012.10.188

also reported to control conductivity [9,10], are affected not only by sintering temperature and time but also by particle size of starting powder. While the positive effect of density on conductivity is well documented, the clear relationship between grain size and conductivity has not been established. Lenka at al. [11] have found that reduced grain size improves conductivity at lower temperatures (<650 °C), whereas conductivity at higher temperature actually decreases with reduction in grain size.

In order to achieve high density at temperature as low as possible it is essential to synthesize nanosized powders with high specific surface and therefore high driving force for sintering. Although there are a plenty of methods that have been used to obtain fine powders, self propagating room temperature synthesis (SPRT) is one of the most cost and time effective methods. It is based on the reaction between metal (Me) nitrates and sodium hydroxide (NaOH) as presented by following equation [12]:

$$2\{(1-x)Ce(NO_3)_3\cdot 6H_2O\}+\{xMe(NO_3)_3\cdot 6H_2O\}+6NaOH+(1/2-\delta)O_2\rightarrow 2Ce_{1-x}Me_xO_{2-\delta}+6NaNO_3+15H_2O \quad (1)$$

The advantage of SPRT method is the possibility of synthesizing nanopowders at room temperature without the need for subsequent calcinations of the obtained powder. Unlike SPRT method, there are synthesis methods such as sol–gel [13,14] or combustion syntheses [15,16] which require subsequent calcination of obtained powders in order to remove the organic components. The calcination step increases production cost and prolongs the time of synthesis. Furthermore, SPRT synthesis normally involves hand mixing of starting materials in an alumina mortar which is quite inconvenient when it comes to larger amounts of powder [17,18].

The intention of this study is to fabricate samarium (Sm)/gadolinium (Gd) co-doped ceria powder using simple ball milling instead of hand mixing. Sm and Gd dopants were chosen as there are a number of studies showing the positive effect of these dopants on electrical conductivity of ceria. Another novelty of this work is related to an improvement of driving force for sintering. It will be shown that almost full dense Sm and Gd co-doped ceria can be fabricated by pressureless sintering of homogenous mixture of Sm doped ceria and Gd doped ceria powders at 1550 °C.

2. Material and methods

2.1. Powder preparation

Starting reactants used in this study were cerium nitrate hexahydrate ($Ce(NO_3)_3\cdot 6H_2O$), samarium nitrate hexahydrate ($Sm(NO_3)_3\cdot 6H_2O$), gadolinium nitrate hexahydrate ($Gd(NO_3)_3\cdot 6H_2O$) and NaOH from Alfa Aesar GmbH, Germany. Amounts of nitrates and NaOH were calculated according to the nominal compositions of solid solutions: $Ce_{0.8}Sm_{0.1}Gd_{0.1}O_{2-\delta}$, $Ce_{0.8}Sm_{0.2}O_{2-\delta}$ and $Ce_{0.8}Gd_{0.2}O_{2-\delta}$. The first batch (I), with composition $Ce_{0.8}Sm_{0.1}Gd_{0.1}O_{2-\delta}$, was made by hand mixing of the reactants in alumina mortar for ~5 min. After an exposure to air for 3 h, the reaction product mixture was rinsed in a centrifuge-Megafuge 1.0, Heraeus, at 3500 rpm to remove $NaNO_3$. This procedure was repeated three times with distilled water and twice with ethanol. The powder was dried at 90 °C. The second batch (II) with composition $Ce_{0.8}Sm_{0.1}Gd_{0.1}O_{2-\delta}$, was prepared in the same way except that 1-h long milling was done in plastic jar with alumina balls. The preliminary experiments showed that milling time of 5 min was too short to provide homogenization of starting reactants. For this reason the milling time was extended to 1 h. Water was used as milling media. The third batch (III) was an equimolar mixture of single doped ceria solutions: $Ce_{0.8}Sm_{0.2}O_{2-\delta}$ and $Ce_{0.8}Gd_{0.2}O_{2-\delta}$.The single doped ceria solutions were prepared similarly to batch II, starting from cerium nitrate, NaOH and corresponding nitrate as a source of dopant. $Sm(NO_3)_3\cdot 6H_2O$ was used to prepare Sm doped ceria, whereas $Gd(NO_3)_3\cdot 6H_2O$ was used to prepare Gd doped ceria. After rinsing and drying, the two single doped ceria powders were mixed by ball milling for 1 h in order to obtain overall composition of $Ce_{0.8}Sm_{0.1}Gd_{0.1}O_{2-\delta}$. The mixture was dried in order to remove milling media (water). It is important to point out the difference between batches II and III. Although the overall compositions of both batches are the same, the distribution of Sm and Gd dopants in powder particles is different. Unlike batch II which consists of particles with uniform composition containing both Sm and Gd dopant, batch III is a mixture of particles containing only Sm and particles containing only Gd. In order to make sample notation easier, both obtained powders and sintered samples will be designated with I, II, III which refers to the route that was used to synthesize powder. Quite often an extended notation will be also used: I (hand mixing of co-doped ceria), II (ball-milling of co-doped ceria) and III (ball milling of single doped ceria powders).

2.2. Compaction and sintering

Green pellets were prepared by mechanical, uniaxial pressing of obtained powders under 60 MPa. Sintering was performed at 1550 °C for 1 h in air. The heating rate was 5°/min.

2.3. Sample characterization

Density of sintered samples was measured by Archimedes method. The relative density was given as a ratio between the measured density and theoretical density which was calculated applying a rule of mixture. The specific surface area of powders was measured by Brunauer–Emmett–Teller (BET) method using N_2 absorption at −196 °C. The phase composition of powders as

well as sintered samples was determined by XRD. The powder particle morphology and microstructure of sintered samples were examined under scanning electron microscopy (SEM). Interception method was used to measure grain size of sintered samples. The chemical composition of grains was determined by energy dispersive X-ray spectroscopy (EDS). Electrical conductivity was measured by impedance spectroscopy method. Platinum paste was applied on both flat sides of the sintered pellets and heated up to 700 °C. The measurements were carried out in temperature range from 250 to 700 °C in air using HP 4194A equipment under 42 Hz–1 MHz frequency. The impedance data were fitted by software Z-View2 (version 2.6 demo).

3. Results and discussion

3.1. XRD analysis of powders

X-ray patterns of powders obtained using the three different routes are presented in Fig. 1. As can be seen, the obtained powders are single phase ceria with fluorite crystal structure. Considerable broadening of X-ray lines implies nanometric crystallite size. It is important to stress that the intensity of diffraction lines of samples obtained by milling (II and III) is higher than that for samples obtained by hand mixing (I) which indicates that milling provides energy sufficiently high to improve diffusion and therefore promote powder crystallization. The highest degree of crystallinity was observed for powder III as a result of an additional 1-h long milling of single-doped ceria powders. The calculation of the crystallite size was performed on the basis of the full width at half maximum intensity (FWHM) of the peak at ~28.5° applying Williamson–Hall method [19]. The values for crystallite size are given in Table 1, which shows that the crystallite size lies in the range 3–6 nm. The smallest value was measured for hand-mixed powder (I) which, again, indicates that milling promotes crystallite growth.

3.2. Specific surface area of powders

The specific surface area was calculated by BET equation based on adsorption and desorption isotherms which are presented in Fig. 2. According to the IUPAC classification [20], the isotherms belong to type-IV with a hysteresis loop which is associated with mesoporous materials. The calculated values for specific surface area are given in Table 1. As expected, hand-mixed powder (I) has the highest specific surface area as a result of the smallest crystallite size (Table 1).

3.3. SEM analysis of powders

Although the SEM analysis of powders was conducted, it was quite difficult to determine the actual particle size from the obtained micrographs due to intensive powder agglomeration. The agglomerates were not broken even after intensive ultrasonic treatment. As Fig. 3 evidences, the morphology of the agglomerates depends on the synthesis route. While the agglomerates in powder obtained by hand mixing are large and fairly porous (Fig. 3a) the agglomerates in powders obtained by ball milling (Fig. 3b and c) are more compacted. The more compacted agglomerate structure can be explained by the solubility of reaction product such as $NaNO_3$ in water, which was used as a milling media. Unlike hand-mixed samples (no water) in which newly created $NaNO_3$ stays

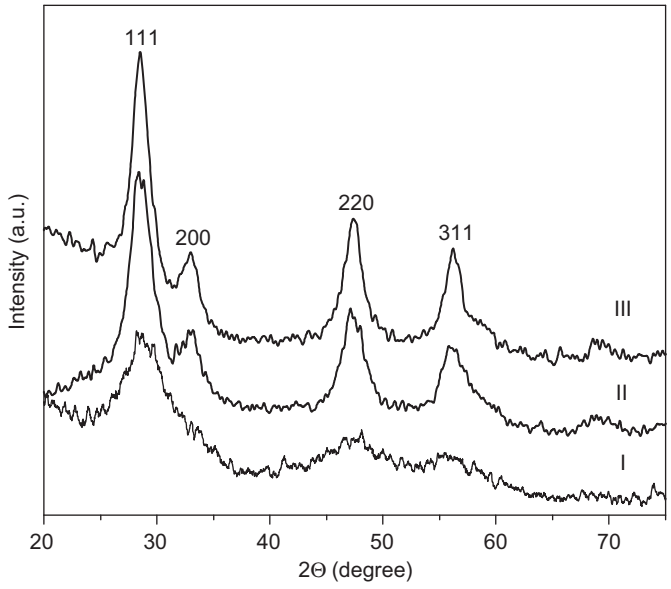

Fig. 1. X-ray diffraction patterns of powders obtained by hand mixing of co-doped ceria (I), ball-milling of co-doped ceria (II) and ball milling of single doped ceria powders (III).

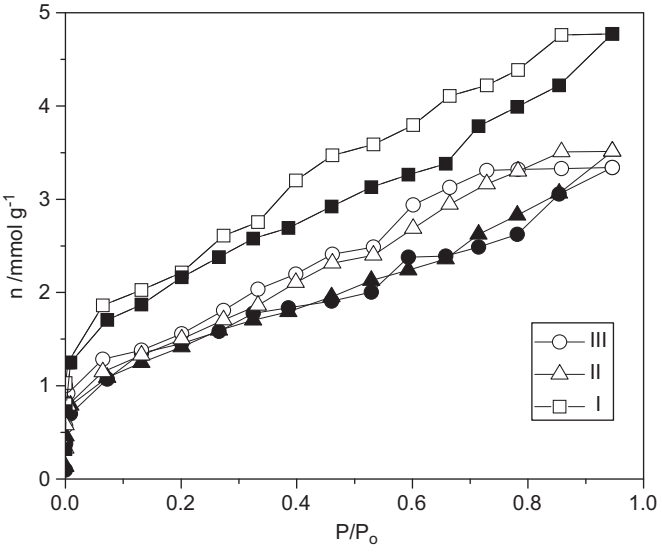

Fig. 2. Nitrogen adsorption and desorption isotherms of powders obtained by: hand mixing of co-doped ceria (I), ball milling of co-doped ceria (II) and ball milling of single doped ceria powders (III). Solid symbols – adsorption, open symbols – desorption.

Table 1
Crystallite size and specific surface area of powders obtained by: hand mixing of co-doped ceria (I), ball milling of co-doped ceria (II) and ball milling of single doped ceria powders (III).

Sample	Crystallite size (nm)	Specific surface area (m^2/g)
I	3.36	144
II	4.36	113
III	5.15	105

evenly dispersed between ceria particles, in ball-milled samples, $NaNO_3$ partially dissolves in water, leaves the space between ceria particles and allows their agglomeration. After drying, the dissolved $NaNO_3$ normally forms $NaNO_3$ rich layer on the top of the powder cake. High porosity as well as specific surface area of agglomerates in hand-mixed sample can be ascribed to rinsing of fine $NaNO_3$ particles evenly dispersed between ceria particles.

3.4. XRD analysis and density of sintered samples

Fig. 4 shows X-ray patterns of samples sintered at 1550 °C for 1 h. As can be seen, all samples are solid solutions of ceria without any trace of secondary phase.

Densities of powder compacts sintered at 1550 °C for 1 h are given in Table 2. It is quite unexpected that the lowest density was measured in sample I which was made of powder with the smallest particle size and therefore with the highest driving force for sintering. It is believed that the low sintering density of sample I is a result of an uneven stress distribution within the green compact. The presence of relatively large, porous, agglomerates in the starting powder obtained by hand mixing simply does not allow an even compaction of the powder resulting in inhomogeneous density of the green samples as well as the sintered samples. Fig. 5 shows high density area surrounded by porous area. Normally, these dense areas contain fairly large cracks which might be formed owing to the presence of tensile stress in the dense areas. The stress is created due to larger shrinkage of dense areas than that of the surrounding, porous, areas. It can be inferred from the above results that the decrease in particle size of powder does not necessarily lead to improved densification.

Another important finding is related to the density of samples obtained by sintering of powders prepared by ball milling (II and III). As Table 2 shows, the density of sample III, which is obtained by sintering of mixture of single doped ceria powders, is higher than that of sample II, which is obtained by sintering of co-doped ceria. It appears that the different composition of powder particles in sample III can enhance mass transport during sintering and thus improve density to above 99%TD. As mentioned, powder III is a mixture of particles containing Sm and particles containing Gd, whereas powder II consists of particles containing both Sm and Gd dopant. Although

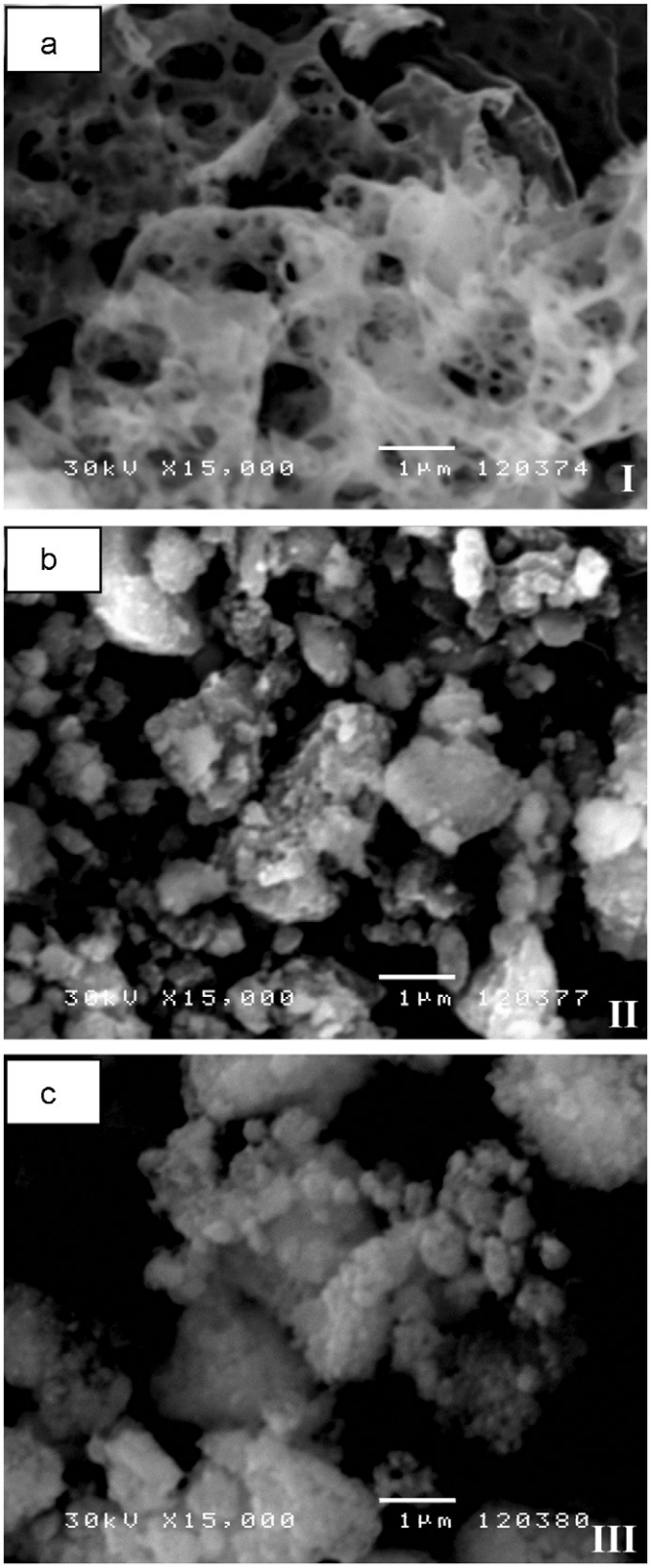

Fig. 3. SEM micrographs of powder samples obtained by: (a) hand mixing of co-doped ceria (I), (b) ball milling of co-doped ceria (II) and (c) ball milling of single doped ceria powders (III).

the chemical composition of particles in powders II and III is not the same, EDS analysis reveals that the chemical composition of grains in sintered samples II and III is the

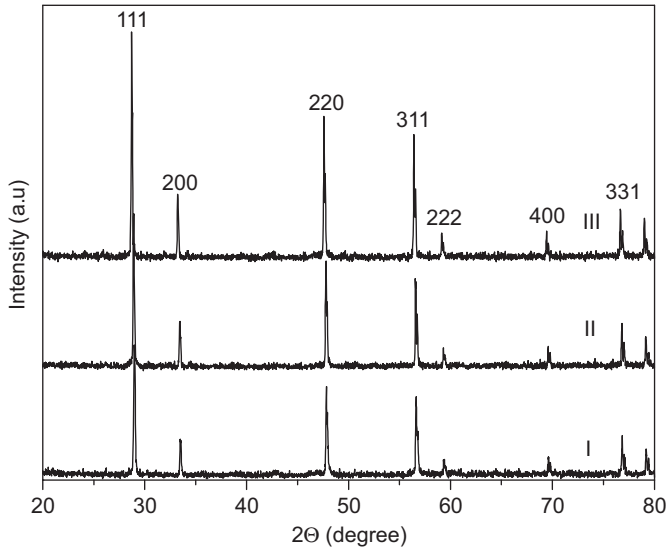

Fig. 4. X-ray patterns of samples sintered at 1550 °C for 1 h. The samples were obtained by sintering of powder prepared by hand mixing of co-doped ceria (I), ball milling of co-doped ceria (II) and ball milling of single doped ceria powders (III).

Table 2
Density and grain size of samples obtained by sintering of powders prepared by: hand mixing of co-doped ceria (I), ball milling of co-doped ceria (II) and ball milling of single doped ceria powders (III).

Sample	Density (%TD)	Grain size (μm)
I	95.3	1.2 ± 0.1
II	98.5	2.1 ± 0.2
III	99.2	1.9 ± 0.2

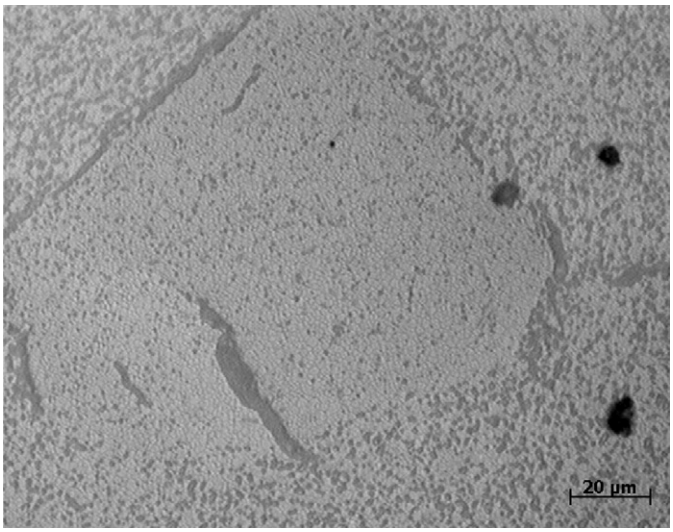

Fig. 5. Dense region surrounded by porous area in sample I (hand mixing of co-doped ceria) sintered at 1550 °C for 1 h.

same (Fig. 6). This indicates that Sm and Gd diffuse between Sm doped ceria and Gd doped ceria particles during sintering of sample III. The result of this diffusion is a uniform distribution of dopants over the volume of sintered sample III. Finally, it would be very important to stress that such high density of samples II and III was achieved without cold isostatic pressing (CIP) which is normally used to further improve green density of mechanically pressed pellets. A direct benefit of elimination of CIP is the fabrication cost reduction.

3.5. SEM analysis of sintered samples

Microstructures of sintered samples are presented in Fig. 7. Fig. 7b and c shows that samples II and III are quite similar regarding porosity and grain size. The figures reveal that both samples have low porosity (high density) and similar grain size. Results of careful measurement of grain size are listed in Table 2. The results evidence that the grain size of sample III is slightly smaller than that of sample II, which was measured to be about 2.1 μm. Furthermore, Fig. 7a reveals that the porosity of sample I is higher than that of samples II and III, whereas the grain size of sample I is considerably smaller (1.2 μm) than that of samples II and III. Although the mechanical properties of ceria electrolyte are not the object of this study it is believed that samples II and III might have better mechanical properties than sample I despite coarser microstructure. It is well known that strength, which is considered as the most important mechanical property, is affected by both grain size and porosity [21]. The effect of grain size is especially pronounced in an anisotropic material in which an increase in grain size is normally followed by a decrease in strength due to residual stresses. However, bearing in mind that ceria is isotropic material (due to cubic crystal structure) it is quite possible that strength is controlled by porosity rather than by grain size. Therefore, samples II and III which have higher density than sample I are expected to have higher strength despite the fact that grain size is larger. In addition, when it comes to comparison of samples II and III it is evident that sample III will have higher strength since density is higher and grain size is somewhat smaller than that in sample II. Careful observation of microstructures of samples II and III reveals that the largest grain in sample III was below 5 μm, whereas grains with diameter of more than 7 μm were observed in sample II.

It can be summarized that samples obtained by sintering of powder prepared by ball milling (II and III) have higher density but larger grain size than samples obtained by sintering of powder prepared by hand mixing (I). When it comes to samples obtained by sintering of powder prepared by ball milling (II and III) it appears that sintering of mixture of single doped ceria powders (III) gives samples with higher density and smaller grain size than sintering of normally used, co-doped, ceria powder (II).

Now, when high density is achieved, it would be of interest to study ionic conductivity of these samples.

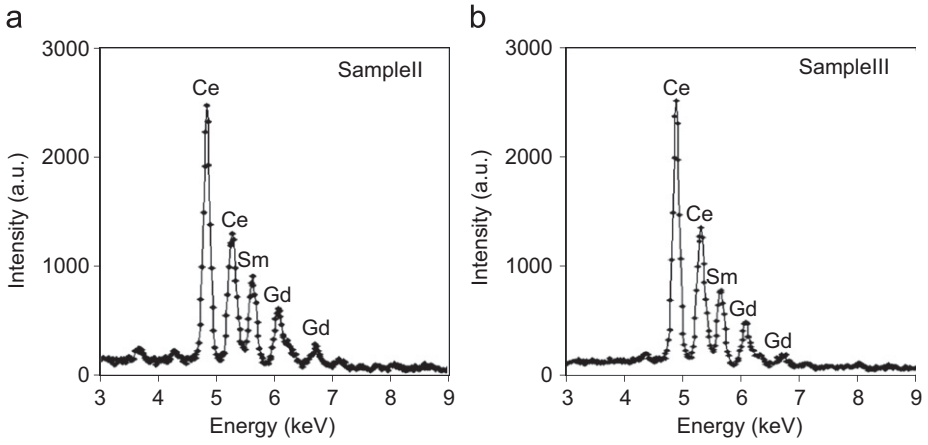

Fig. 6. EDS spectra of samples sintered at 1550 °C for 1 h. The samples were obtained by sintering of powder prepared by (a) ball milling of co-doped ceria (II) and (b) ball milling of single doped ceria powders (III). The spectra were recorded in the middle of grains.

3.6. Conductivity

The impedance spectra measured at 300 and 600 °C are presented in Fig. 8. The horizontal axis refers to the real resistance, whereas the vertical axis refers to the imaginary resistance. The spectra were interpreted using the equivalent electrical circuits. The impedance spectra measured at 300 °C were well simulated by the equivalent circuit consisting of a series of one resistance (R), two parallel circuits of resistance and capacitance (C) and Warburg impedance (W) (Fig. 8a). The incomplete semicircle in the high frequency range is normally attributed to the migration of oxygen ions in the bulk, i.e., bulk resistivity. Very often it is simulated by parallel connected resistance ($R1$) and capacitor ($C1$). However, in this study, a good match between the measured spectra and the spectra of proposed circuit was obtained by adding another resistance ($R2$). It was found that careful variation of $R2$ changes the shape of the high frequency semicircle and therefore bulk resistivity which may be roughly determined from the right intercept of the semicircle and horizontal axis (real resistance). Although it is quite difficult to determine the phenomenon to which $R2$ element corresponds it is believed that $R2$ is related to the pore presence. This reasoning was supported by the impedance spectra given in Fig. 8a showing that the high frequency semicircle of sample I (sample with the highest porosity) is slightly wider than those of samples II and III indicating that the bulk resistance of sample I is also slightly higher than that of samples II and III. Unlike the high frequency semicircle which appears only partially in the limited frequency range of equipment (≤ 1 MHz), the middle range frequency semicircle is complete. In this case the parallel connected resistance ($R3$) and capacitor ($C2$) are used to model the experimental data. The middle range frequency semicircle corresponds to the migration of oxygen ions across the grain boundary and very often is used to determine both the grain bulk resistance and the grain boundary resistance. The left intercept of grain boundary semicircle and the horizontal axis represents the bulk resistivity, whereas the distance between the left and the right intercept represents the grain boundary resistivity. As Fig. 8a indicates the grain boundary resistivity of sample I is considerably higher than those of samples II and III. The increased grain boundary resistivity is considered to be the result of small grain size and thus increased fraction of grain boundaries. Therefore the total resistivity from the bulk and grain boundary is the highest for sample I.

Finally, the origin of the low frequency semicircle was simulated by Warburg impedance ($W1$), which corresponds to the sample/electrode interfacial impedance. This impedance is associated with formation of oxygen ions at the interface through reaction: $O_2 + 4e^- \rightarrow 2O^{2-}$.

The impedance spectra measured at 600 °C are presented in Fig. 8b. At such high temperature the semicircles are shifted to the frequencies higher than 1 MHz, which are out of the range of equipment. Therefore the total resistivity from the bulk and grain boundary is measured based on the intercept of electrode semicircle and the horizontal axis. As expected, the total resistivity of sample I is higher than that of samples II and III. Again, the smaller grain size and higher porosity of sample I are considered to be the reason for higher total resistance of sample I at 600 °C. Furthermore, Dusastre et al. [22] proposed another way to verify that the semicircles which appear in the impedance spectra are associated with the grain bulk and grain boundary resistance. This evaluation is based on the capacitance (C') which can be obtained for each semicircle using following equation:

$$C' = \frac{1}{2\pi f R'} \tag{2}$$

Where f is the frequency at the semicircle maximum and R' is the resistance (Z_{Re}) at the semicircle maximum. They have found that the values of C' for grain boundary response were typically from 7 to 25 nF, whereas the capacitance values for grain bulk were from 30 to 60 pF. In this study, the values of C' for the middle range

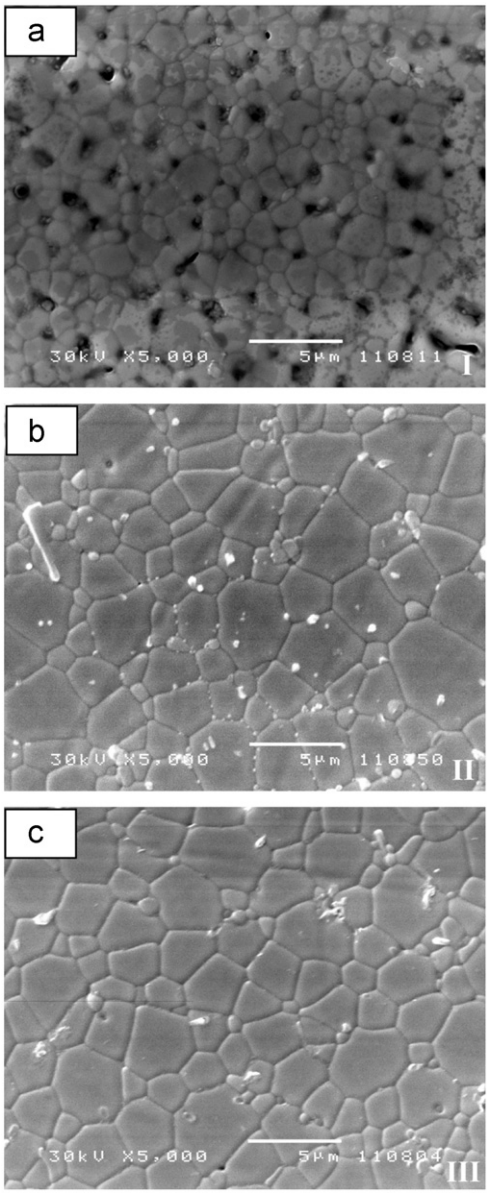

Fig. 7. SEM micrographs of polished and etched surface of samples sintered at 1550 °C for 1 h. The samples were obtained by sintering of powders prepared by (a) hand mixing of co-doped ceria (I), (b) ball milling of co-doped ceria (II) and (c) ball milling of single-doped ceria powders (III). The surface of samples contains impurities which fell of the wall of the tube furnace during thermal etching.

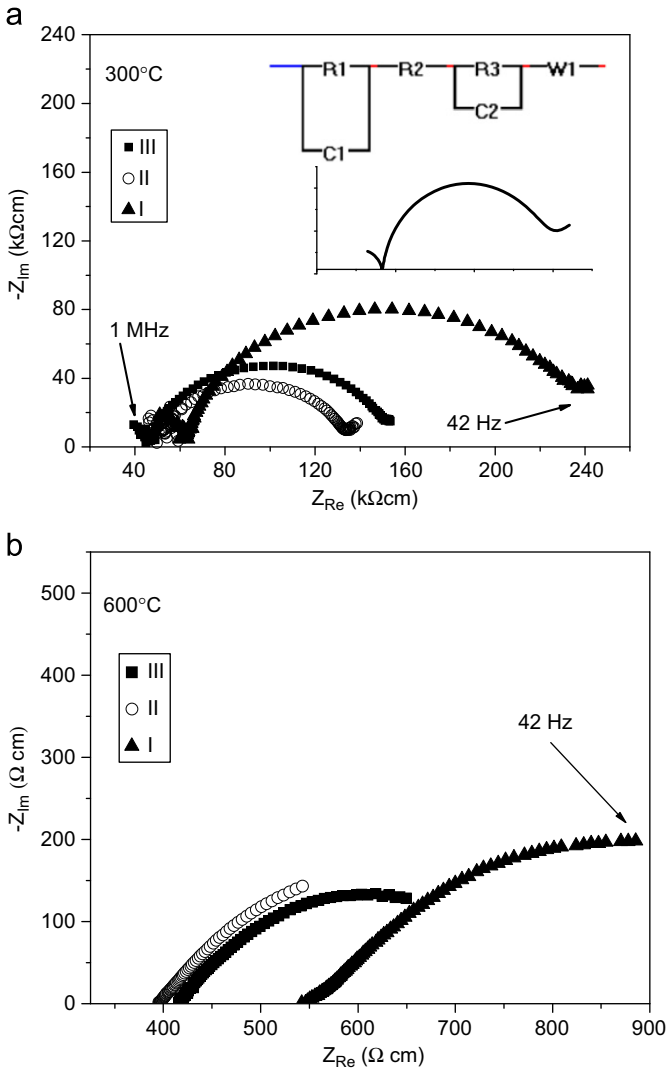

Fig. 8. Complex impedance spectra of samples obtained by sintering of powder prepared by hand mixing of co-doped ceria (I), ball milling of co-doped ceria (II) and ball milling of single doped ceria powders (III) measured at (a) 300 °C and (b) 600 °C. The inserted diagram in Fig. 8a presents the fitted spectra of corresponding equivalent circuit.

frequency semicircle for samples I, II and III (Fig. 8a) are calculated to be 0.3, 1.3 and 1.9 nF, respectively. The calculated values of C' are very close to the expected values for grain boundary response which confirms that the middle range frequency semicircle in the impedance spectra measured at 300 °C is associated with the grain boundary resistance.

The measured values of total resistivity were used to calculate the total conductivity in temperature range 250–700 °C.

Fig. 9. presents the change of total conductivity with temperature in the form of Arrhenius plots. The graphs were plotted based on Nernst–Einstein equation [23]

$$\ln \sigma T = \ln \sigma_o - \frac{E_a}{RT} \tag{3}$$

where σ is the total conductivity, T is the temperature, σ_o is the constant associated with the frequency factor of migration of oxide ions, E_a is the activation energy of migration of oxide ions and R is the gas constant. The figure shows that the coarse-grained samples II and III have higher conductivity than the fine-grained sample I. However, it is quite difficult to distinguish the effect of grain size on conductivity from the effect of porosity. Bearing in mind that the density of sample I is lower than that of samples II and III it is expected that the porosity present in sample I decreases its conductivity. This is also supported by the study conducted by Jo et al. [9], which showed that porosity can considerably reduce

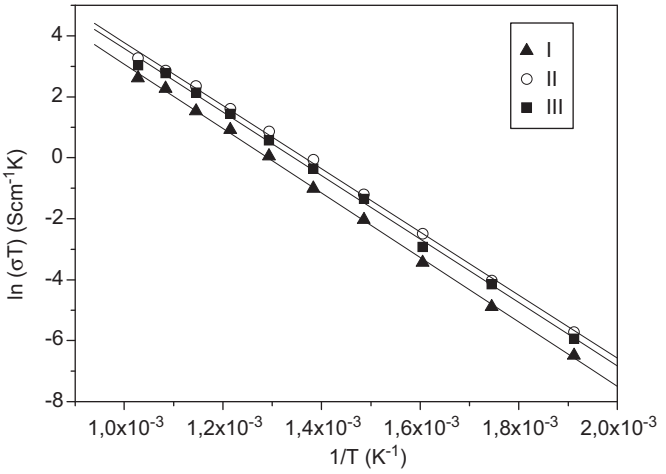

Fig. 9. Arrhenius plots of total conductivity of samples sintered at 1550 °C for 1 h. The samples were obtained by sintering of powder prepared by: hand mixing of co-doped ceria (I), ball milling of co-doped ceria (II) and ball milling of single doped ceria powders (III).

the conductivity of fine-grained ceria. When it comes to the dense samples II and III it can be seen that the conductivity of sample II is somewhat higher than that of sample III, which has slightly smaller average grain size than sample II. It appears that in this system, an increase in grain size leads to an increase in the total conductivity due to reduction in grain boundary fraction and consequent increase in the grain boundary conductivity. The activation energy of migration of oxide ions, Ea, was calculated based on the slope of linear fit of conductivity values given in Fig. 9. The results show that the highest Ea of 87.9 kJ/mol was calculated for sample I, whereas the lowest Ea of 86.1 kJ/mol was calculated for sample II. Very small difference in activation energy of different samples suggests that pre-exponential factor σ_o (Eq. 3), which is associated with the frequency factor of migration of oxide ions, might be responsible for the lower conductivity of sample I. According to Eq. 3, the decrease in pre-exponential factor σ_o results in the decrease in ionic conductivity. It is quite expected that the frequency factor of migration of oxide ions in porous sample I is smaller than that of dense samples II and III. The considerable porosity present in sample I simply reduces the actual cross section area available for the oxide ion migration.

4. Conclusions

Ball milling is an effective way to fabricate dense samples of co-doped ceria, ($Ce_{0.8}Sm_{0.1}Gd_{0.1}O_{2-\delta}$) using SPRT method. The samples obtained by ball milling had higher density, larger grains size and higher conductivity than samples obtained by hand mixing. Even higher density can be achieved by sintering the mixture of single-doped ceria powders ($Ce_{0.8}Sm_{0.2}O_{2-\delta}$ and $Ce_{0.8}Gd_{0.2}O_{2-\delta}$). It appears that uneven distribution of dopants improves densification and slightly inhibits grain growth. It was found that in system such this, the electrical conductivity increases with an increase in grain size.

Acknowledgments

This work has been supported by the Ministry of Education and Science of Serbia (project number: 45012).

References

[1] B.C. Steele, A. Heinzel, Materials for fuel-cell technologies, Nature 414 (2001) 345–352.
[2] S. Kuharuangrong, Ionic conductivity of Sm, Gd, Dy and Er-doped ceria, Journal of Power Sources 171 (2007) 506–510.
[3] X. Sha, Z. Lu, X. Huang, J. Miao, Z. Ding, X. Xin, W. Su, Study on La and Y co-doped ceria-based electrolyte materials, Journal of Alloys and Compounds 428 (2007) 59–64.
[4] J.X. Zhu, D.F. Zhou, S.R. Guo, J.F. Ye, X.F. Hao, X.Q. Cao, J. Meng, Grain boundary conductivity of high purity neodymium-doped ceria nanosystem with and without the doping of molybdenum oxide, Journal of Power Sources 174 (2007) 114–123.
[5] H. Inaba, H. Tagawa, Ceria-based solid electrolytes, Solid State Ionics 83 (1996) 1–16.
[6] R.K. Lenka, T. Mahata, A.K. Tyagi, P.K. Sinha, Influence of grain size on the bulk and grain boundary conductivity behaviour in gadolinia-doped ceria, Solid State Ionics 181 (2010) 262–267.
[7] T. Mori, J. Drennan, J.H. Lee, J.G. Li, T. Ikegami, Oxide ionic conductivity and microstructures of Sm- or La-doped CeO_2-based systems, Solid State Ionics 154-155 (2002) 461–466.
[8] H.J. Avila-Paredes, K. Choi, C.T. Chen, S. Kim, Dopant-concentration dependence of grain-boundary conductivity in ceria: A space-charge analysis, Journal of Materials Chemistry 19 (2009) 4837–4842.
[9] S.H. Jo, P. Muralidharan, D.K. Kim, Electrical characterization of dense and porous nanocrystalline Gd-doped ceria electrolytes, Solid State Ionics 178 (2008) 1990–1997.
[10] D.S. Kim, P.S. Cho, J.H. Lee, D.Y. Kim, S.B. Lee, Improvement of grain-boundary conduction in gadolinia-doped ceria via post-sintering heat treatment, Solid State Ionics 177 (2006) 2125–2128.
[11] R.K. Lenka, T. Mahata, A.K. Tyagi, P.K. Sinha, Influence of grain size on the bulk and grain boundary ion conduction behavior in gadolinia-doped ceria, Solid State Ionics 181 (2010) 262–267.
[12] S. Boskovic, D. Djurovic, Z. Dohcevic-Mitrovic, Z. Popovic, M. Zinkevich, F. Aldinger, Self-propagating room temperature synthesis of nanopowders for solid oxide fuel cells, Journal of Power Sources 145 (2005) 237–242.
[13] C.D.E. Lakeman, D.A. Payne, Sol-gel processing of electrical and magnetic ceramics, Materials Chemistry and Physics 38 (1994) 305–324.
[14] L.C. Klein, Sol–gel processing of ionic conductors, Solid State Ionics 32–33 (1989) 639–645.
[15] T. Mahata, G. Das, R.K. Mishra, D.P. Sharma, Combustion synthesis of gadolinia doped ceria powder, Journal of Alloys and Compounds 391 (1-2) (2005) 129–135.
[16] B. Matovic, D. Bucevac, N. Jiraborvornpongsa, K. Yoshida, T. Yano, Synthesis and characterization of nanometric strontium-doped ceria solid solutions via glycine-nitrate procedure, Journal of the Ceramic Society of Japan 120 (2) (2012) 69–73.
[17] B. Matovic, Z. Dohcevic-Mitrovic, M. Radovic, Z. Brankovic, G. Brankovic, S. Boskovic, Z.V. Popovic, Synthesis and characterization of ceria based nanometric powders, Journal of Power Sources 193 (1) (2009) 146–149.
[18] X. Yu, F. Li, X. Ye, X. Xin, Z. Xue, Synthesis of cerium(IV) oxide ultrafine particles by solid-state reactions, Journal of the American Ceramic Society 83 (4) (2000) 964–966.
[19] B. Lonnberg, Characterization of milled Si_3N_4 powder using X-ray peak broadening and surface area analysis, Journal of Materials Science 29 (12) (1994) 3224–3230.
[20] K.S.W. Sing, D.H. Everett, R.A.W. Haul, L. Moscou, R.A. Pierotti, J. Rouquerol, T. Siemieniewska, Reporting physisorption data for

gas/solid systems with special reference to the determination of surface area and porosity, Pure and Applied Chemistry 57 (1985) 603–619.
[21] V.D. Krstic, Effect of microstructure on fracture of brittle materials: unified approach, Theoretical and Applied Fracture Mechanics 45 (2006) 212–226.
[22] V. Dusastre, J.A. Kilner, Optimisation of composite cathodes for intermediate temperature SOFC applications, Solid State Ionics 126 (1999) 163–174.
[23] P.G. Shewnon, Diffusion in Solids, New York, McGrew-Hill Book Company, 1963 286-287.